AFRL-AFOSR-UK-TR-2024-0011

Nonreciprocity in Integrated Optical and Microwave Optomechanical Based Systems

Kippenberg, Tobias
Ecole Polytechnique Fédérale de Lausanne
Bâtiment CE 3316 Station 1
Lausanne, VD, , 1015
CH

12/12/2023
Final Technical Report

Air Force Research Laboratory
Air Force Office of Scientific Research
European Office of Aerospace Research and Development
Unit 4515 Box 14, APO AE 09421

REPORT DOCUMENTATION PAGE

PLEASE DO NOT RETURN YOUR FORM TO THE ABOVE ORGANIZATION.

1. REPORT DATE	2. REPORT TYPE	3. DATES COVERED	
20231212	Final	START DATE 20191201	END DATE 20231130

4. TITLE AND SUBTITLE
Nonreciprocity in Integrated Optical and Microwave Optomechanical Based Systems

5a. CONTRACT NUMBER	5b. GRANT NUMBER	5c. PROGRAM ELEMENT NUMBER
	FA8655-20-1-7009	
5d. PROJECT NUMBER	**5e. TASK NUMBER**	**5f. WORK UNIT NUMBER**

6. AUTHOR(S)
Tobias Kippenberg

7. PERFORMING ORGANIZATION NAME(S) AND ADDRESS(ES)
Ecole Polytechnique Fédérale de Lausanne
Bâtiment CE 3316 Station 1
Lausanne, VD 1015
CH

8. PERFORMING ORGANIZATION REPORT NUMBER

9. SPONSORING/MONITORING AGENCY NAME(S) AND ADDRESS(ES)	10. SPONSOR/MONITOR'S ACRONYM(S)	11. SPONSOR/MONITOR'S REPORT NUMBER(S)
EOARD UNIT 4515 APO AE 09421-4515	AFRL/AFOSR IOE	AFRL-AFOSR-UK-TR-2024-0011

12. DISTRIBUTION/AVAILABILITY STATEMENT
A Distribution Unlimited: PB Public Release

13. SUPPLEMENTARY NOTES

14. ABSTRACT
During this program, we reported acousto-optic modulation of a silicon nitride micro-resonator utilizing high-overtone bulk acoustic wave resonances (HBAR), where the acoustic wave penetrates vertically towards the substrate. Although HBAR is frequently used in contemporary communication, sensors, and superconducting circuits, this was the first time it was used on a photonic integrated chip. To enhance the electromechanical and optomechanical coupling efficiency, we focused our efforts on fabricating hybrid integrated released MEMS-photonic devices. This was achieved by releasing Si substrate below the actuators, leaving a thin acoustic cavity mainly consisting of the silicon oxide cladding embedding the silicon nitride waveguides, which led to the demonstration of magnet-free optical isolation via angular momentum biasing. Secondly, we have recently proposed and comprehensively analyzed a new kind of transducer harnessing the strong piezoelectric coupling of microwave signals to a mechanical excitation, a high overtone bulk acoustic resonance (HBAR), parametrically interacting with optical super-modes of optically coupled ring cavities to realize a coherent microwave-optical conversion. This device takes advantage of the high-quality factors of silicon nitride waveguides fabricated using the photonic damascene process. The integration of micro-electro-mechanical (MEMS) actuators on top of these waveguides allows for modulation using stress-optical phenomena, namely the moving boundaries and photoelastic effects. An important step in the modular approach to quantum computing can be made possible by improvements to these transducers, such as grounding for cryogenic compatibility and release process optimization, which would also make it much easier to build up quantum networks.

15. SUBJECT TERMS

16. SECURITY CLASSIFICATION OF:			17. LIMITATION OF ABSTRACT	18. NUMBER OF PAGES
a. REPORT	b. ABSTRACT	c. THIS PAGE		
U	U	U	SAR	8

19a. NAME OF RESPONSIBLE PERSON	19b. PHONE NUMBER *(Include area code)*
ATTILA SZEP	314 235 6044

Standard Form 298 (Rev.5/2020)
Prescribed by ANSI Std. Z39.18

“Nonreciprocity in integrated optical and microwave optomechanical based systems”

AFOSR-MURI Final Performance Report

Prof. Tobias J. Kippenberg
Swiss Federal Institute of Technology Lausanne (EPFL)
Laboratory of Photonics and Quantum Measurements

Period of Performance: 01.12.2019 – 30.11.2023

Award N° FA8655-20-1-7009
EUROPEAN OFFICE OF AEROSPACE RESEARCH AND DEVELOPMENT
Program Manager: Dr. Attila Szep, AFOSR/IOE

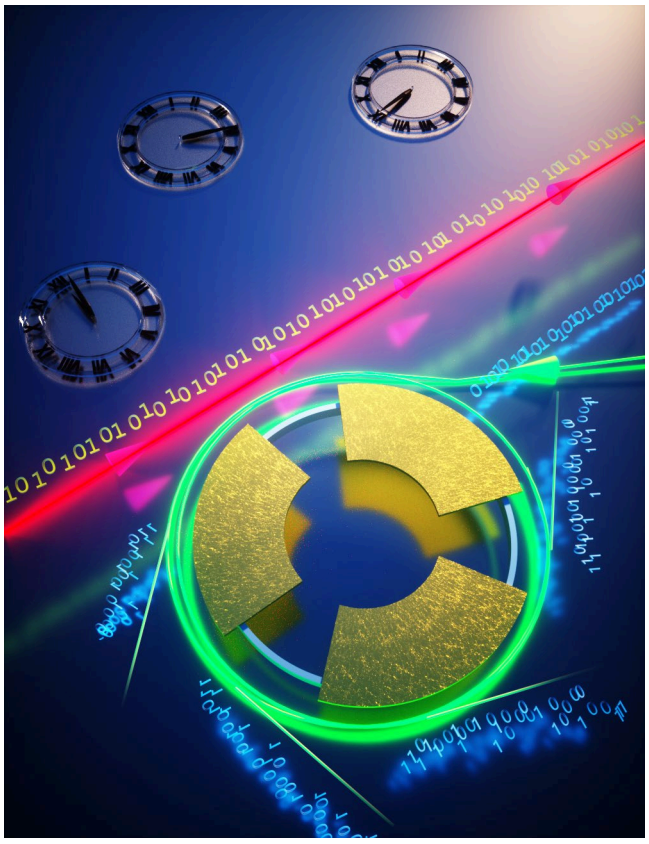

Figure 1: Artistic illustration of magnet-free optical isolator based on hybrid piezo-optomechanical nanophotonic device.

1. Abstract

During this program, we reported acousto-optic modulation of a Si_3N_4 microresonator utilizing high-overtone bulk acoustic wave resonances (HBAR) [1], where the acoustic wave penetrates vertically towards the substrate. Although HBAR is frequently used in contemporary communication, sensors, and superconducting circuits, this was the first time it was used on a photonic integrated chip. To enhance the electromechanical and optomechanical coupling efficiency, we focused our efforts on fabricating hybrid integrated released MEMS-photonic devices. This was achieved by releasing Si substrate below the actuators, leaving a thin acoustic cavity mainly consisting of the SiO_2 cladding embedding the Si_3N_4 waveguides, which led to the demonstration of magnet-free optical isolation via angular momentum biasing [2].

Secondly, we have recently proposed and comprehensively analyzed a new kind of transducer [3] harnessing the strong piezoelectric coupling of microwave signals to a mechanical excitation, a high overtone bulk acoustic resonance (HBAR), parametrically interacting with optical supermodes of optically coupled ring cavities to realize a coherent microwave-optical conversion. This device takes advantage of the high-quality factors of Si_3N_4 waveguides fabricated using the photonic damascene process [4]. The integration of MEMS actuators on top of these waveguides [5] allows for modulation using stress-optical phenomena, namely the moving boundaries and photoelastic effects. An important step in the modular approach to quantum computing can be made possible by improvements to these transducers, such as grounding for cryogenic compatibility and release process optimization, which would also make it much easier to build up quantum networks.

2. List of accomplishments during this period

2.1 Released Hybrid nanophotonic high-overtone bulk acoustic resonator (HBAR) platform

In our previous work [1], by integrating aluminum nitride (AlN) piezoelectric actuators on top of Si_3N_4 photonic devices, we demonstrated the first acousto-optic modulation (AOM) of Si_3N_4 microring resonators using HBARs. Sub-micrometer wavelength acoustic waves are excited by macroscopic actuators, which transmit vertically into the substrate and perpendicular to optical paths. Moving further, we concentrated our efforts on enhancing the modulation efficiency. Optomechanical single-photon coupling strength g_0 is inversely proportional to the square root of the mode volume of the mechanical and optical modes. The efficiency is proportional to the square of g_0, thus making efficiency proportional to the inverse of the mechanical mode volume. Also, the electromechanical coupling efficiency increases by shrinking the mode volume due to better impedance match [6]. Hence, to enhance the modulation efficiency, we partially release the optical microring from its silicon substrate, thereby reducing the volume of the HBAR modes to a small region where it interacts with the optical field. This improves the energy transfer from the microwave control to the optical signal to the point that modes residing in the silicon oxide cladding can now be detected optically.

Figure 1d shows the fabricated device's false-colored, top-view scanning electron microscope (SEM) image with three AlN actuators integrated on a released Si_3N_4 microring resonator. The thickness of Al / AlN / Mo is 100 / 1000 / 100 nm, respectively. The center hole is opened for Si-isotropic dry etching using the SF_6 Bosch process, to partially remove the Si substrate and to suspend the 5.4-µm-thick SiO_2 cladding. Figure 1b shows the simulated stress distribution of one HBAR mode within the SiO_2 layer using Finite Element Method (FEM). It can be seen that the HBAR mode is uniformly distributed under the AlN actuator and tightly confined in the SiO_2 membrane, allowing direct modulation of the optical mode propagating along the waveguide through photoelastic and moving boundary effects.

The measured microwave reflection S_{11} spectrum as shown in Figure 1c shows a distinct feature with a free spectral range of approximately 350 MHz that coincides with the peaks appearing on the optical transmission spectrum S_{21}. This response shows a large signal-to-noise ratio (SNR) that is significantly higher in magnitude as compared to the response of bulk devices. The small resonances from Si substrate HBAR as presented in

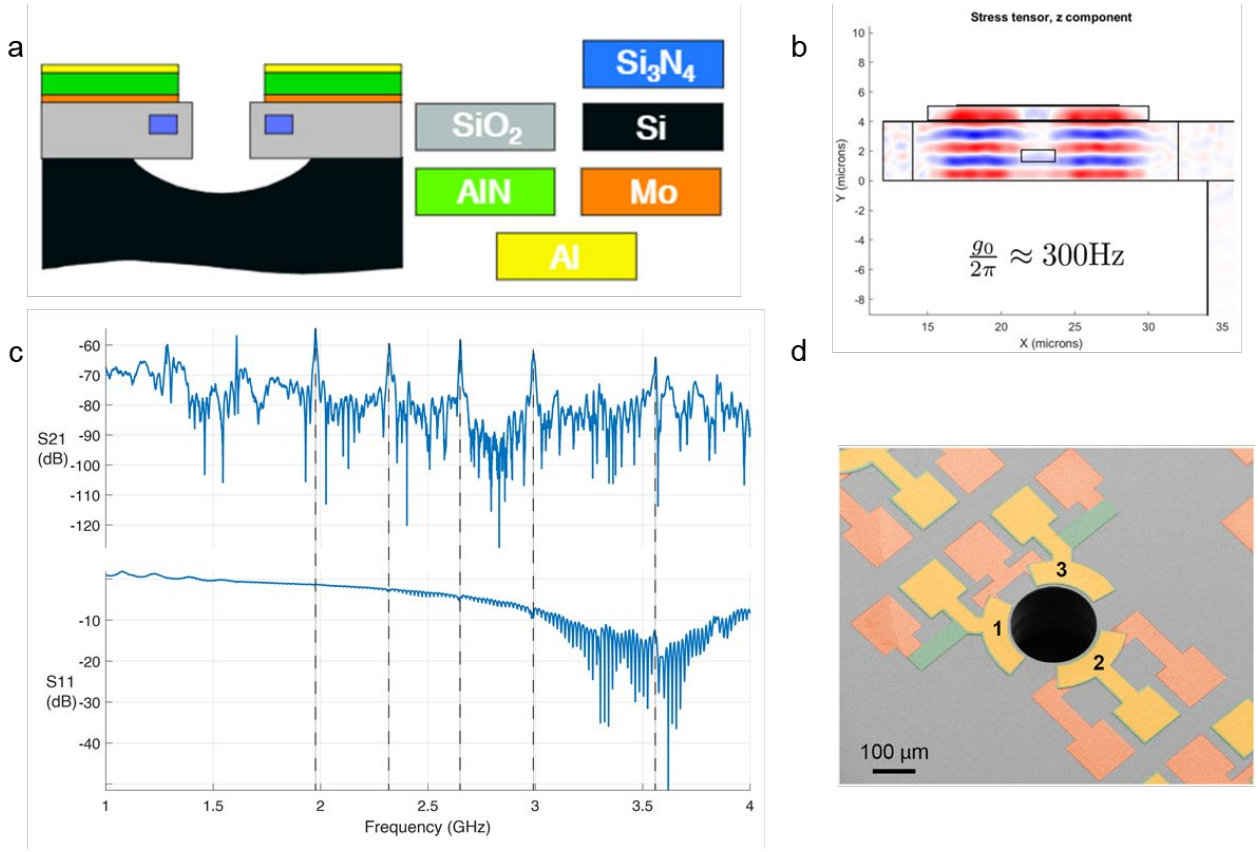

Figure 2: Characterization of mechanical properties of the integrated MEMS-photonic device. (a) Schematic showing suspended SiO2 membrane containing the Si3N4 microring resonator, to enhance the optomechanical coupling. The key technique used here is the Si isotropic dry etch using SF6 Bosch process (b) FEM numerical simulations of the vertical stress σz distribution of a typical HBAR mode at 3 GHz. (c) Optomechanical S21 response of an actuator and its microwave reflection S11. (d) False-colored top-view SEM image of the fabricated device.

S_{11} are significantly reduced in the optical transmission S_{21}, since the Si HBAR is mainly located at the outer anchor region that is far away from the inner Si_3N_4 ring.

2.2 Magnet-free nitride optical isolator

Spatiotemporal modulation [7], [8], stands out in terms of integration and application on almost all optical materials because it breaks reciprocity by connecting two optical modes and imposing phase matching conditions through active modulation. Here, we demonstrate the first AOM-based optical isolator for Si_3N_4 integrated photonics. By synchronously driving multiple piezoelectric MEMS actuators, bulk acoustic waves are generated electromechanically, which can couple to and deflect light propagating in the Si_3N_4 waveguide beneath them. While magnetic-free optical isolators have been shown before, this is the first one that is driven electrically and operated in the linear optical regime.

The Si_3N_4 microresonator is designed to support two optical eigenmodes, *a* and *b*, with frequency differences matching a mechanical/acoustic resonant frequency, as shown in 2b. The microwave drive applied on the three AlN actuators creates acoustic waves inside the mechanical cavity, which scatters light between modes *a* and *b* (i.e. indirect interband transition). 2c illustrates the ω-k space. To induce interband transition, energy and momentum conservations must be satisfied. With a nonzero phonon momentum k_m, phase matching requires $\Delta\omega_{ba} = \omega_b - \omega_a = \Omega_m$ and $\Delta k_{ba} = k_b - k_a$. In the forward direction, the two optical modes undergo interband transition with a scattering rate $g = g_0\sqrt{n_c}$, where g_0 is the single phonon-photon coupling rate describing the optomechanical interaction strength, and n_c is the steady-state intra-cavity phonon number.

$C = 4g^2/\kappa_a\kappa_b$ is the optical-to-optical cooperativity, which measures the ratio of scattering rate to optical losses. Strong coupling requires $C >> 1$, and can lead to Rabi oscillation and mode splitting. The latter results in a transparency window on the resonance in the light transmission in the forward direction. In the backward direction where the three-wave phase matching is not fulfilled, the interband transition is prohibited, leading to $C << 1$ and transmission is zero in the critical coupling regime. This non-reciprocal transmission between the forward ($T = 1$) and backward directions ($T = 0$) is the basis of our optical isolator.

We use the high efficiency of the undercut HBAR to demonstrate magnet-less optical isolator by breaking reciprocity via spatiotemporal modulation. We achieve an optical cooperativity C = 1 with 14 dBm RF drive power applied on each actuator, and maximum isolation ratio of 10 dB and a minimum insertion loss of 0.1 dB with 20 dBm RF power. An isolation bandwidth of 700 MHz is obtained, primarily determined by the optical resonance linewidth. Hence, to demonstrate a greater isolation ratio with larger bandwidth, we use an over-coupled device, achieving 41 dB isolation and 1.9 dB insertion loss under 2-Watt total RF power.

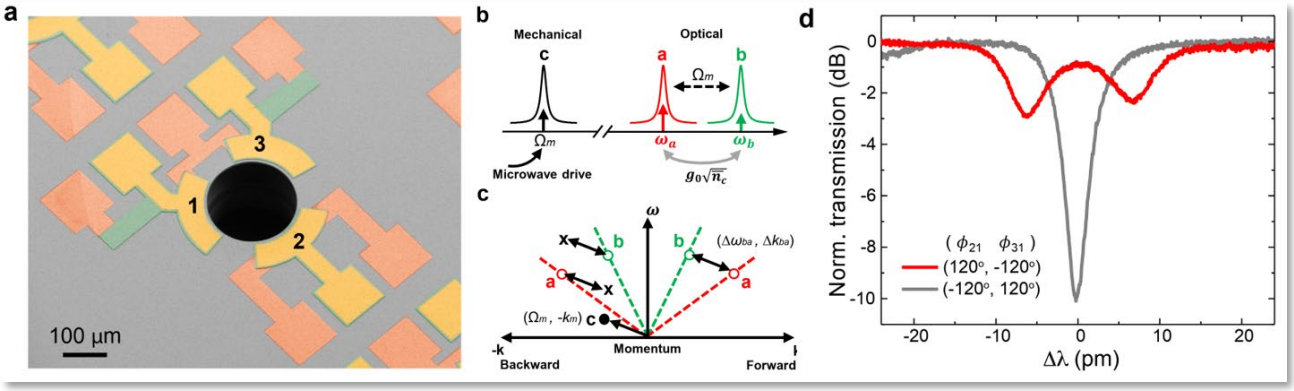

Figure 3: Optical isolator via spatiotemporal modulation (a) A false-colored top-view SEM image of the fabricated device. (b) A frequency-domain representation illustrating the indirect interband transition. (c) A schematic of ω-k space showing the phase matching condition, that is, the energy and momentum conservations. (d) Optical transmission spectra with perfect phase matching (red) and largest phase mismatch (grey).

2.3 Bidirectional microwave-optical transduction based on integration of high-overtone bulk acoustic resonators and photonic circuits

Coherent interconversion between microwave and optical frequencies can serve as both classical and quantum interfaces for computing [9], communication, and sensing. Here, we present a compact microwave-optical transducer based on monolithic integration of piezoelectric actuators atop silicon nitride photonic circuits [2]. Such an actuator directly couples microwave signals to a high-overtone bulk acoustic resonator defined by the suspended silica cladding of the optical waveguide core, which leads to enhanced electromechanical and optomechanical couplings. At room temperature, this triply resonant piezo-optomechanical transducer achieves an off-chip photon number conversion efficiency of 1.6×10^{-5} over a bandwidth of 25 MHz at an input pump power of 21 dBm. The approach is scalable in manufacturing and, unlike existing electro-optic transducers, does not rely on superconducting resonators. As the transduction process is bidirectional, we further demonstrate synthesis of microwave pulses from a purely optical input. Combined with the capability of leveraging multiple acoustic modes for transduction, the present platform offers prospects for building frequency-multiplexed qubit interconnects and for microwave photonics at large [10].

We measure the off-chip efficiency η^{tot} of the microwave-to-optical (up-conversion) and optical-to-microwave (down-conversion) processes as a function of off-chip CW input optical pump power P_{in}. Compared to the on-chip efficiency η^{oc}, this efficiency also accounts for the loss channels of the microwave and optical ports. First, we study the transducer in the triply resonant configuration. For up-conversion, the optical sideband generated

from the microwave input, detuned by $\omega_{in} = \omega_m$ from the pump frequency, is measured via a self-calibrated heterodyne detection method. The off-chip optical output containing both the pump (ω_L) and the sideband (ω_s)

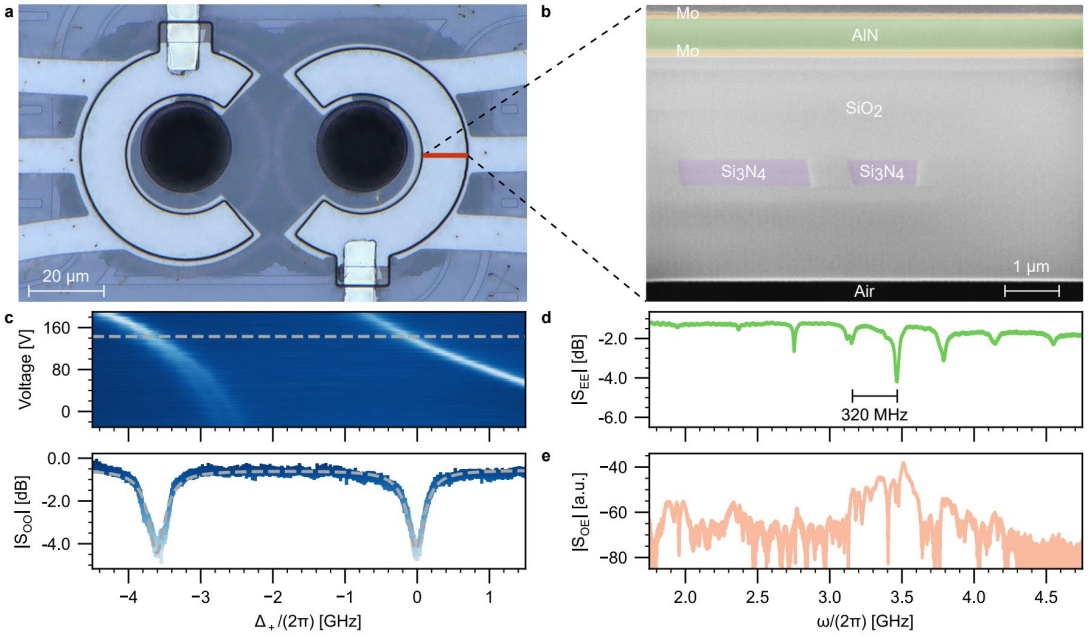

Figure 4: Device metrological and network characterization. (a) Optical micrograph of the transducer. The shaded region originates from the released silicon substrate. (b) False-color cross section of the device imaged by focused ion beam scanning electron microscopy showing the top and bottom electrodes (Mo; yellow), piezoelectric layer (AlN; green), suspended cladding (SiO_2; gray), and optical waveguides (Si3N4; purple). (c) Optical transmission spectra near 1550 nm as a function of applied DC piezoelectric control voltage and detuning from the antisymmetric supermode. The transmission color map follows the representative spectrum in the bottom panel. The dashed line denotes the best-fit transmission to coupled mode theory. (d) Microwave reflection spectrum indicating locations of the HBARs. (e) Acousto-optic response spectrum with an off-chip optical pump power Pin = 16 dBm centered at the symmetric supermode.

is combined with a local oscillator (LO; ω_{LO}) and detected. By placing the LO at a frequency $\omega_{LO} = (\omega_L + \omega_s)/2 + \delta$ such that the photodetector response is constant over a frequency span of δ, we determine the sideband power relative to the pump. Picking off a fraction of the optical output then enables the determination of its absolute power and, by extension, that of the sideband with a power meter. The measured optical sideband power is compared to that of the microwave input to yield η^{tot}. In the case of down-conversion, the optical input is generated by modulating the phase of the pump with an electrooptic modulator (EOM) driven by a microwave source of frequency $\omega_{EOM} = \omega_m$. Only one of the resulting sidebands is admitted into the photonic molecule and transduced, as the other is far off-resonance. Summarized in Figs. 4a and c, bidirectional transduction processes corresponding to both the effective beam-splitter ($\omega_L = \omega_-$; anti-Stokes) and two-mode-squeezing ($\omega_L = \omega_+$; Stokes) interactions are investigated. We reach a maximal η^{tot} of −48 dB at 21 dBm pump for each configuration. Knowing the port losses, we estimate an on-chip efficiency $\eta^{oc} = -41$ dB. Accounting for the extraction efficiency η^{ext}, we further obtain an internal conversion efficiency $\eta^{int} = 2 \times 10^{-3}$.

Furthermore, we deviate from triple resonance to map out the transduction bandwidth. First, for a pump still resonant with one of the optical supermodes, the input microwave frequency ω_{in} and input optical detuning (controlled by EOM drive frequency ω_{EOM}) are varied for up- and down-conversion, respectively. Shown in Fig. 4b and d, transduction leveraging the main transduction mode exhibits a full width at half maximum (FWHM) of 25 MHz. The multimode nature of the transducer is further manifest in Fig. 4e, where the pump is in the beam-splitter configuration but slightly detuned from $\hat{a}_-$. An additional transduction peak in η^{tot} with a FWHM of 10 MHz is observed around $\omega_{in} = 2\pi \times 3.165$ GHz, which corresponds to another HBAR one FSR away from the main transduction mode $\omega_m = 2\pi \times 3.480$ GHz. The engineering degrees of freedom such as

cladding and actuator thickness (HBAR FSR), and optical dispersion (supermode splitting as a function of optical wavelength) in the present system offer possibilities for frequency multiplexed transduction.

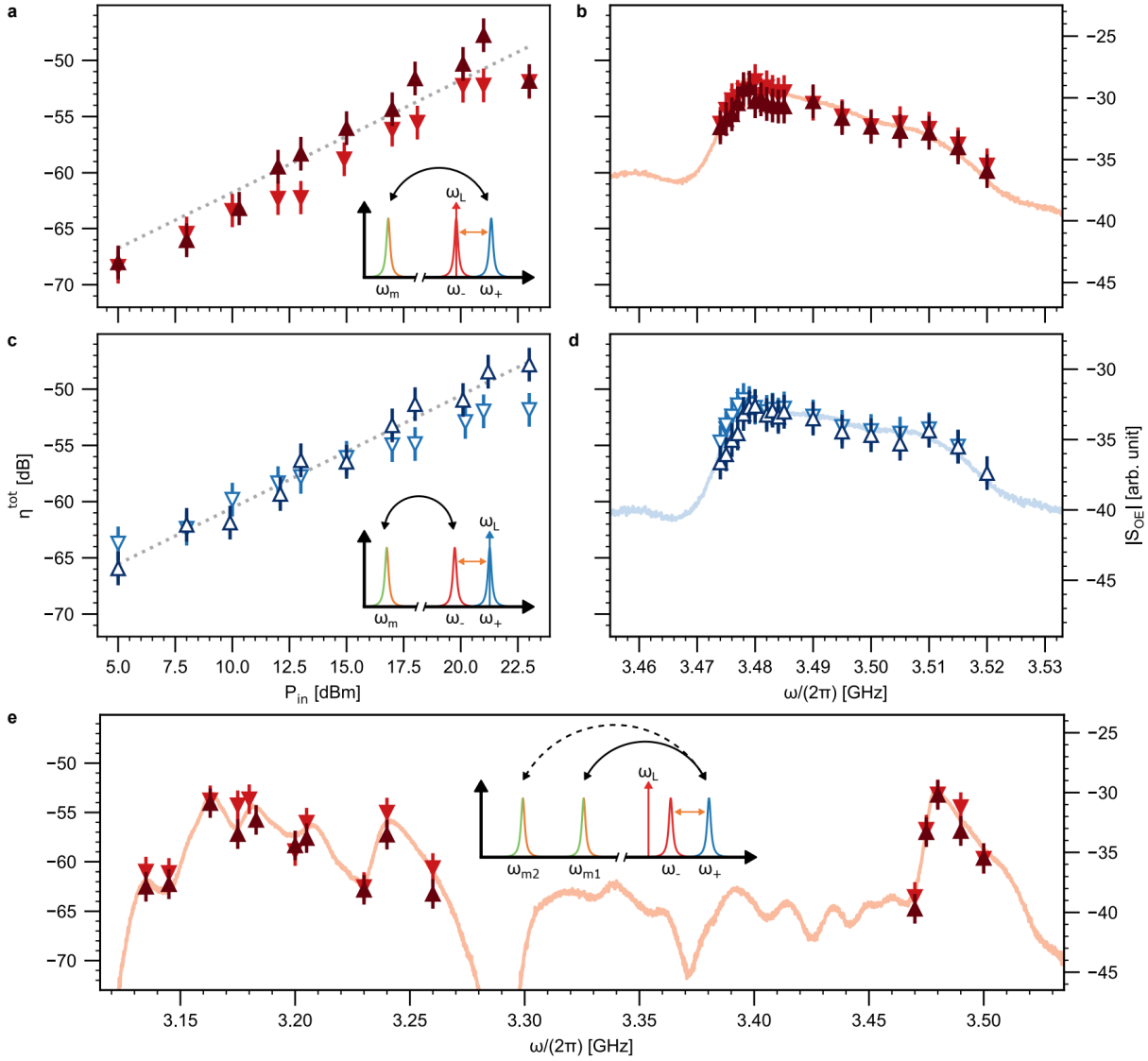

Figure 5: Bidirectional, multimode transduction with a continuous-wave pump. (a), (b) Anti-Stokes transduction. (c), (d) Stokes transduction. Off-chip efficiencies as a function of off-chip input pump power in the triply resonant configuration are shown in the left panels. Off-chip efficiencies as a function of input microwave frequency and input optical detuning are plotted in the right panels, which depict the transduction bandwidth. (e) Bidirectional transduction with a detuned pump leveraging multiple HBAR modes, as a function of input microwave frequency and input optical detuning. Up- and down-conversion efficiencies are denoted by triangles and inverted triangles, respectively, with the corresponding acoustic-optic response spectrum superimposed. The markers are empty for Stokes processes and filled for anti-Stokes processes. The dotted lines represent the best-fit efficiency in the low-cooperativity regime where $\eta_{tot} \propto C \propto P_{in}$. The insets illustrate the respective configurations for both the pump and input signal.

2.4 Pull-back fabrication process of piezoactuator electrodes

The "Pull-back process" for fabrication of electrodes is engineered to minimize the capacitance of bond-pads and for the ease of wire-bonding to the bond-pads and thereby helping in impedance matching with the microwave. As shown in Figure 5a, we start with a layer stack of top Mo, AlN, and bottom Mo on top of the SiO_2. We have used deep reactive-ion etching to pattern the Mo and AlN layers. Prior to the pullback process, the top-electrode bond pad had a layer of AlN and bottom Mo underneath it, creating a capacitor. Given the

width of the bond pad is more than double the width of the device itself, the capacitance added is significant and should be avoided to reduce the RC time constant. We can eliminate the capacitance by etching through the top Mo, AlN, and bottom Mo layers and depositing a layer of Al to connect the top electrode bond pad.

However, the deposited Al must be electrically isolated from the bottom Mo. Thus, we add the "Pull-back" step for which the process is named to create an air gap between the top and bottom metals. XeF_2 etches Mo but has a near infinite selectivity with AlN. Therefore, using an isotropic etching process, the Mo can be slightly etched away without harming the AlN.

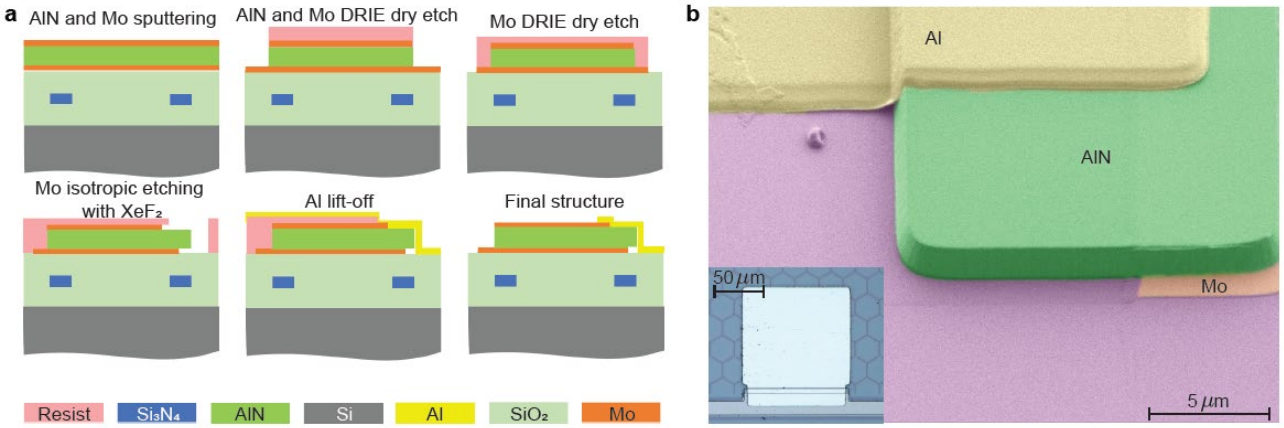

Figure 6: Pull-back fabrication process. (a) Process flow of the fabrication. (b) False-colored SEM image of the electrodes fabricated by this fabrication technique. The inset is a photograph taken by an optical microscope of the top electrode.

We "Pull-back" the Mo from underneath the AlN between 1 and 2 μm, and then deposit a layer of Al with a lift-off process. A glancing angle deposition tool evaporates 200 nm of Al with a 15^0 angle on a rotating plate to make sure the Al covers the 1 μm AlN step height. The final result is a gap of air between the bottom Mo and top Al leaving them electrically isolated, but Al is electrically connected to the top Mo layer. Figure 6(b) shows a trial of this technique, and it can be seen that the Mo has been pulled back from underneath the AlN and the Al has been deposited on top and fully covers the step height of the AlN. In this trial, Al served as the entire top metal without top Mo, however the device described in this work has a layer of top Mo between the Al and AlN layers.

3. Publications

[1] H. Tian, J. Liu, A. Siddharth *et al.*, "Magnetic-free silicon nitride integrated optical isolator," ***Nat. Photonics***, vol. 15, no. 11, pp. 828–836, Nov. 2021, doi: 10.1038/s41566-021-00882-z.

[2] Tian, H., Liu, J., Dong, B. et al. "Hybrid integrated photonics using bulk acoustic resonators", ***Nat Commun*** 11, 3073 (2020), doi: 10.1038/s41467-020-16812-6.

[3] T. Blésin, W. Kao, A. Siddharth, *et al.*, "Bidirectional Microwave-Optical Transduction Based on Integration of High-Overtone Bulk Acoustic Resonators and Photonic Circuits", arXiv:2308.02706.

Other related work

[1] T. Blésin, H. Tian, S. A. Bhave, and T. J. Kippenberg, "Quantum coherent microwave-optical transduction using high-overtone bulk acoustic resonances," ***Phys. Rev. A***, vol. 104, no. 5, p. 052601, Nov. 2021, doi: 10.1103/PhysRevA.104.052601.

[2] Liu, J., Tian, H., Lucas, E. et al. "Monolithic piezoelectric control of soliton microcombs", ***Nature*** 583, 385–390 (2020), doi: 10.1038/s41586-020-2465-8.

4. Conference proceedings

[1] Anat Siddharth, Terence Blesin, Hao Tian, Wenle Weng, Rui Ning Wang, Junqiu Liu, Sunil A. Bhave, and Tobias J. Kippenberg, "Optical Gyrator and Microwave-to-Optical Converter using HBAR modes", CLEO US (2021 and CLEO Europe 2021.

[2] H. Tian, J. Liu, A. Siddharth, Terence Blesin, T. J. Kippenberg and S. A. Bhave, "X-band AOM on chip", IEEE MEMS (January 2021).

[3] H. Tian, J. Liu, C. Skehan, A. Siddharth, T. J. Kippenberg and S. A. Bhave, "A Nitride Ring Isolator", **CLEO (2020)**.

[4] H. Tian, D. Bin, M. Zervas, J. Liu, T. J. Kippenberg and S. A. Bhave, "Stress-Optical Modulator Using Bulk Acoustic Resonant Vibrations", **IFCS-EFTF (2019)**.

[5] Terence Blésin, Anat Siddharth, et al, "Microwave-optical transduction using high overtone bulk acoustic resonances", **APS March Meeting (2022), IFCS-EFTF (2022), CLEO (2022), ECIO (2022)**.

[6] Terence Blésin, Wil Kao, Anat Siddharth, et al, "Bidirectional microwave-optical transduction based on bulk acoustic resonators-silicon nitride integrated photonics co-integration", **IBM Quantum Transduction Workshop (2023)**.

5. List of supported students

Ph.D. student: Anat Siddharth, Terence Blésin

References

[1] H. Tian *et al.*, "Hybrid integrated photonics using bulk acoustic resonators," *Nature Communications*, vol. 11, no. 1, Art. no. 1, Jun. 2020, doi: 10.1038/s41467-020-16812-6.

[2] H. Tian *et al.*, "Magnetic-free silicon nitride integrated optical isolator," *Nat. Photon.*, vol. 15, no. 11, pp. 828–836, Nov. 2021, doi: 10.1038/s41566-021-00882-z.

[3] T. Blésin, H. Tian, S. A. Bhave, and T. J. Kippenberg, "Quantum coherent microwave-optical transduction using high-overtone bulk acoustic resonances," *Phys. Rev. A*, vol. 104, no. 5, p. 052601, Nov. 2021, doi: 10.1103/PhysRevA.104.052601.

[4] J. Liu *et al.*, "High-yield, wafer-scale fabrication of ultralow-loss, dispersion-engineered silicon nitride photonic circuits," *Nat Commun*, vol. 12, no. 1, p. 2236, Apr. 2021, doi: 10.1038/s41467-021-21973-z.

[5] J. Liu *et al.*, "Monolithic piezoelectric control of soliton microcombs," *Nature*, vol. 583, no. 7816, Art. no. 7816, Jul. 2020, doi: 10.1038/s41586-020-2465-8.

[6] T. Blésin, H. Tian, S. Bhave, and T. J. Kippenberg, "Quantum coherent microwave-optical transduction using high overtone bulk acoustic resonances," *arXiv:2103.00471 [quant-ph]*, Mar. 2021, Accessed: Mar. 21, 2021. [Online]. Available: http://arxiv.org/abs/2103.00471

[7] Z. Yu and S. Fan, "Complete optical isolation created by indirect interband photonic transitions," *Nature Photon*, vol. 3, no. 2, pp. 91–94, Feb. 2009, doi: 10.1038/nphoton.2008.273.

[8] Y. Shi, Q. Lin, M. Minkov, and S. Fan, "Nonreciprocal Optical Dissipation Based on Direction-Dependent Rabi Splitting," *IEEE J. Select. Topics Quantum Electron.*, vol. 24, no. 6, pp. 1–7, Nov. 2018, doi: 10.1109/JSTQE.2018.2814792.

[9] "Control and readout of a superconducting qubit using a photonic link | Nature." https://www.nature.com/articles/s41586-021-03268-x (accessed Sep. 19, 2023).

[10] A. P. Higginbotham *et al.*, "Harnessing electro-optic correlations in an efficient mechanical converter," *Nature Phys*, vol. 14, no. 10, Art. no. 10, Oct. 2018, doi: 10.1038/s41567-018-0210-0.